Pekka Alitalo, Stanislav Maslovski, and Sergei Tretyakov. 2006. Experimental verification of the key properties of a three-dimensional isotropic transmission-line superlens. Journal of Applied Physics, volume 99, number 12, 124910.

Experimental verification of the key properties of a three-dimensional isotropic transmission-line superlens

Pekka Alitalo,[a] Stanislav Maslovski,[b] and Sergei Tretyakov[c]
Radio Laboratory/SMARAD, Helsinki University of Technology, P.O. Box 3000, FI-02015 TKK, Finland

(Received 9 January 2006; accepted 23 March 2006; published online 28 June 2006)

Design and experimental realization of a three-dimensional superlens based on inductively and capacitively loaded transmission lines are presented. Transmission properties of the designed structure are studied experimentally and the observed lens properties are compared with analytical predictions. Backward-wave propagation and amplification of evanescent waves in the prototype structure are verified both analytically and experimentally. Commercially available components and materials are used in the design. © *2006 American Institute of Physics*. [DOI: 10.1063/1.2206709]

I. INTRODUCTION

Conventional optical systems make use of refraction and reflection phenomena for image formation. In these systems imaging takes place in the far zone of the source field, in other words, only the far field of the source reaches the imaging instrument. Because the far field is composed only by propagating waves of a certain wavelength, the resolution of a conventional imaging system is always limited.

Although the information about tiny details of the source is lost in the far field, it is present in the near field. Outside the source, its near field can be expressed as a superposition of plane waves. The plane waves that carry the information about small details (smaller than the wavelength) of the source are evanescent waves and they are not present in the far field due to the exponential attenuation that they experience. The scanning optical microscopes use small probes positioned at distances of about a wavelength from the source in order to pick up those quickly decaying fields.

Until recently it seemed impossible to combine the far field and near field imaging principles in a single device. A possibility came into sight after Pendry[1] discovered that negative refraction of electromagnetic waves in a slab of a backward-wave (BW) material (Veselago medium[2]) makes this slab a theoretically perfect lens. He found that the evanescent waves tunnel through the slab with an increase in the amplitude. The rate of this increase is such that it exactly compensates the decay that the evanescent waves undergo on their way from the source to the slab and from the back side of the slab to the image plane. Thus, the focused propagating waves as well as the enhanced evanescent waves of the source sum up in the image plane which yields a theoretically perfect image.

The physics of the amplification of evanescent waves in Pendry's lens was understood as the result of resonant excitation of a coupled pair of surface modes (plasmon polaritons) on the lens surfaces. Later, other systems capable of negative refraction and amplification of evanescent waves were proposed. These systems do not require the use of BW media.[3,4]

Successful demonstrations of negative refraction in a BW material have been done using arrays of resonant cells, which are comprised of metal wires providing effective negative permittivity and split-ring resonators (SRRs) providing effective negative permeability.[5–7] This structure is essentially an artificial uniaxial crystal and therefore is highly anisotropic. The frequency band in which the phase velocity of electromagnetic waves in this structure is negative (the BW regime) is limited by the width of the resonance in SRRs. Also, such systems cannot be made enough dense to allow for effective implementations at radio frequencies. This is why other ways to realize BW materials have been extensively studied in the recent literature.

Another approach to the realization of BW materials is based on *LC*-loaded transmission-line networks.[8–10] These networks do not rely on resonant response from particular inclusions, and the periods of the structures can be made very small as compared to the wavelength. This allows realization of broadband and low-loss devices, which would be extremely difficult if resonant inclusions were used.

So far the transmission-line (TL) network approach has been successfully realized in one and two dimensions,[10–12] and the main challenge on the route towards truly three-dimensional broadband and low-loss superlenses is the realization of isotropic three-dimensional artificial BW structures. In our recent paper we introduced a three-dimensional (3D) isotropic *LC*-loaded transmission-line network and derived the dispersion equation and characteristic impedance of such a network.[13] Also a three-dimensional forward-wave (FW) network was studied. The FW network is similar to the BW network but it does not include the loading elements.[13] Also other ways to design three-dimensional FW and BW transmission-line structures have been proposed.[14,15]

The goal of this paper is to show that the three-dimensional structure analytically described earlier[13] can be practically manufactured using commercially available components, and that this structure possesses the two basic properties of Pendry's superlens, namely, backward-wave propagation and amplification of evanescent waves.

[a]Electronic mail: pekka.alitalo@tkk.fi
[b]Electronic mail: stanislav.maslovski@gmail.com
[c]Electronic mail: sergei.tretyakov@tkk.fi

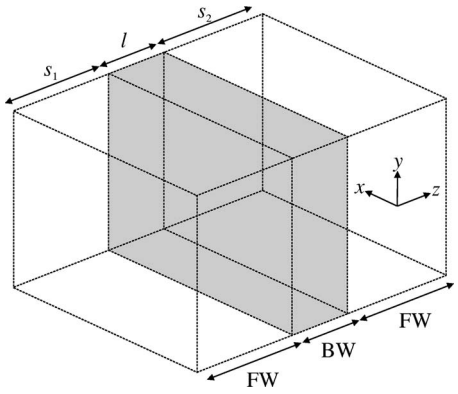

FIG. 1. A three-dimensional superlens with a parallel-sided BW slab surrounded by two FW regions.

II. THE DESIGNED STRUCTURE

The backward-wave network that we use in the lens has been proposed and theoretically studied in Ref. 13. It is a three-dimensional cubic mesh of interconnected transmission-line segments. Every segment is a microstrip line loaded in the middle by a capacitor connected in series with the strip. Those segments form network branches. At the joint points where six neighboring segments intersect, the strips (and, respectively, grounds) are soldered altogether forming a node. Every node is shunted by an inductor to the ground.

In the network the energy propagates through the segments of microstrip lines. Because of the loading elements the waves of voltages and currents at the nodes and the branches are backward in a certain frequency band. From the other hand, the waves in the microstrip line segments in between the loading elements are the usual forward waves. These waves are "hidden" in the lines because of the screening effect of the ground conductor. The complete superlens structure consists of a BW network sandwiched in between two FW networks. The FW networks model free-space regions and are simple unloaded meshes of microstrip lines.[13] See Figs. 1 and 2 for the general geometry of the structure and for the microstrip line unit cells.

The components used in the designed 3D TL-based superlens and its main parameters are listed in Table I. The structure is aimed to work at frequencies around 1 GHz. The period of the structure (d) has to be much smaller than the wavelength (λ) at this frequency. Accordingly, the period is chosen to be 13 mm (the free-space wavelength λ_0 at 1 GHz is 300 mm). For the ease of manufacturing, the thickness of

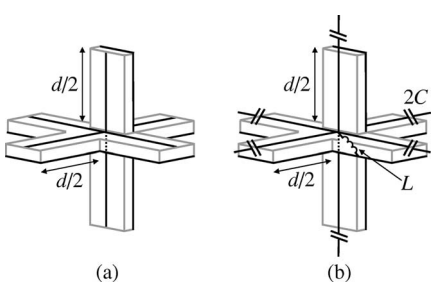

FIG. 2. (a) Unit cell of a 3D FW network. (b) Unit cell of a 3D BW network. d is the period of the network.

TABLE I. Parameters of the prototype and its components.

	Value	Tolerance	Manufacturer	Q factor or loss tangent
d	13 mm	⋯	⋯	⋯
$Z_{0,\mathrm{TL,FW}}$	66 Ω	⋯	⋯	⋯
$Z_{0,\mathrm{TL,BW}}$	89 Ω	⋯	⋯	⋯
C	3.3 pF	±0.05 pF	ATC	$Q_{C,1\ \mathrm{GHz}}=500$
L	6.8 nH	±0.136 nH	ATC	$Q_{L,1\ \mathrm{GHz}}=50$
Substrate	$\varepsilon_r=2.33$	±0.02	Rogers	$\tan\delta=0.0012$

the BW slab (l) has been decided to be three periods, i.e., $l=3d=39$ mm. Using the equations for the characteristic impedances,[13] suitable impedance values of the TLs have been found to be $Z_{0,\mathrm{TL,FW}}=66\ \Omega$ (impedance of the TLs in the FW region) and $Z_{0,\mathrm{TL,BW}}=89\ \Omega$ (impedance of the TLs in the BW region). With these values the characteristic impedances of the FW and BW networks are approximately equal at frequencies near 1 GHz. The height of the substrate is 0.787 mm (Rogers RT/Duroid 5870, $\varepsilon_r=2.33$, thickness of the metallization 35 μm). The lumped elements, i.e., the capacitors and inductors, have been supplied by the American Technical Ceramics Corp. (ATC).

The strip widths (w) and the effective permittivities ($\varepsilon_{r,\mathrm{eff}}$) of the microstrip lines are found from the required impedance values (66 and 89 Ω). The results for the FW network are $w_{\mathrm{FW}}\approx 1.437$ mm, $\varepsilon_{r,\mathrm{eff,FW}}\approx 1.902$, and for the BW network $w_{\mathrm{BW}}\approx 0.794$ mm, $\varepsilon_{r,\mathrm{eff,BW}}\approx 1.845$.

The dispersion equations and characteristic impedances of the FW and BW networks are derived in Ref. 13 and due to their complexity they are not repeated here. By plotting the dispersion curves of the FW and BW networks, one can see that the matching frequency, at which the effective refraction index of the BW region equals -1, is $f\approx 0.8996$ GHz, see Fig. 3(a) (the point where dispersion curves intersect). From Fig. 3(a) it is also seen that at the matching frequency the absolute value of the normalized longitudinal wave number ($k_z d$) is approximately 0.5909 (in both FW and BW regions), which corresponds to the longitudinal wave number $k_z=0.5909/d\approx 45.5\ \mathrm{m}^{-1}$. This is equal to the maximum transverse wave number ($k_t=\sqrt{k_x^2+k_y^2}$) that a propagating wave can have, and therefore we can conclude that for evanescent waves $k_t>45.5\ \mathrm{m}^{-1}$. The maximum transverse wavenumber for evanescent waves is at the edge of the first Brillouin zone: $k_{t,\max}=\pi/d\approx 242\ \mathrm{m}^{-1}$. By plotting the characteristic impedances (Z_0) for the FW and BW networks, one can see that the characteristic impedances of the two networks are approximately equal at the design frequency ($f\approx 0.8996$ GHz), see Fig. 3(b).

III. TRANSMISSION PROPERTIES OF THE DESIGNED STRUCTURE

The equation for the transmission coefficient of the BW slab (T_{lens}) as a function of the transverse wave number k_t was derived earlier,[13] and the result was

$$T_{\text{lens}}(k_t) = \frac{4Z_{0,\text{FW}}(k_t)Z_{0,\text{BW}}(k_t)}{[Z_{0,\text{FW}}(k_t) + Z_{0,\text{BW}}(k_t)]^2 e^{+jk_{z,\text{BW}}(k_t)l} - [Z_{0,\text{FW}}(k_t) - Z_{0,\text{BW}}(k_t)]^2 e^{-jk_{z,\text{BW}}(k_t)l}}, \quad (1)$$

where we assume that the lens axis is parallel to the z axis. The total transmission from the source plane to the image plane is then (the distance from the source plane to the lens is s_1, and the distance from the lens to the image plane is s_2)[13]

$$T_{\text{tot}}(k_t) = T_{\text{lens}}(k_t)e^{-jk_{z,\text{FW}}(k_t)(s_1+s_2)}. \quad (2)$$

To estimate the performance of the designed superlens, the total transmission from the source plane to the image plane can be plotted using Eqs. (1) and (2), see Fig. 4(a), where we have used $s_1=s_2=19.5$ mm and $l=39$ mm. Losses have been neglected in Fig. 4(a).

Tuning the frequency, imaging can be improved, effectively enhancing the transmission of the modes with $k_t > 45.5$ m^{-1} (i.e., evanescent waves). This is due to a better matching of the characteristic impedances at those values of k_t that correspond to evanescent waves. For example, in the lossless case at $f=0.91$ GHz the absolute value of the transmission coefficient $|T_{\text{tot}}|$ is practically equal to unity (and phase equal to zero) for all transverse wavenumbers in the range $0 \leqslant k_t \leqslant k_{t,\max}$. The effect of dissipation caused by the substrate and the lumped components can be considered by taking into account the loss tangent ($\tan\delta$) of the substrate and the quality factors (Q) of the lumped components (shown in Table I), see Fig. 4(b) for this case. As is seen from Fig. 4(b), the transmission properties of this lossy structure are close to the ideal case: $|T_{\text{tot}}| \approx 1$ and $\arg(T_{\text{tot}}) \approx 0$ for a wide range of k_t which includes propagating as well as evanescent spectral components.

IV. TWO-DIMENSIONAL PROTOTYPE

First, in order to check the principles of operation of the proposed structure, a two-dimensional prototype was built (see Fig. 5). The prototype had the same properties and component values as shown in Table I. The edges of the structure were terminated with resistive loads that were approximately matched to the TL impedances. This was done in order to reduce reflections of the propagating modes from the edges of the structure.

The structure was excited by coaxial feeds using SMA (SubMiniature version A) connectors. The feeds were connected to the edge of the first FW region, as shown in the bottom of Fig. 5. To have a possibility to change the position of the excitation, four SMA connectors were soldered to the structure. The inner conductors of the SMA connectors were

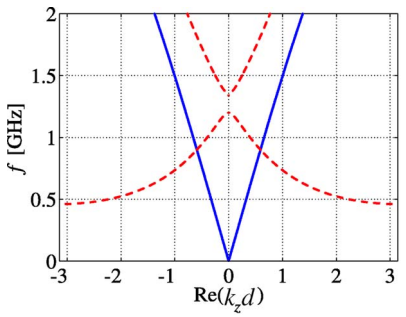

(a)

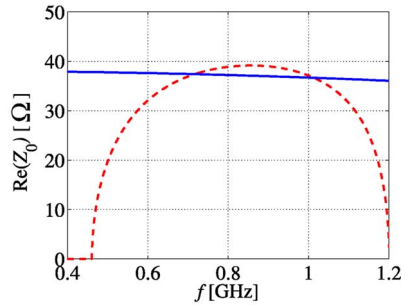

(b)

FIG. 3. (Color online) (a) Dispersion curves of the FW and BW networks (ideal, lossless components). (b) Characteristic impedances of the FW and BW networks (ideal, lossless components). Propagation along the z axis is considered. Solid lines: FW network, dashed lines: BW network.

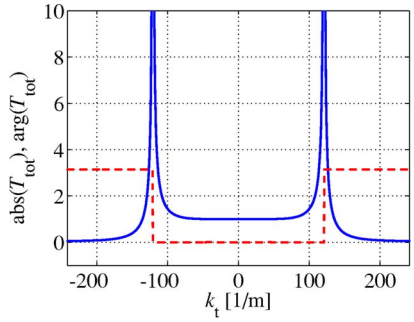

(a)

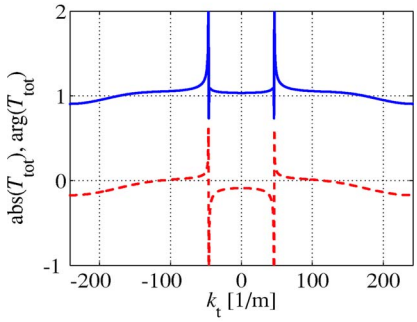

(b)

FIG. 4. (Color online) Absolute value (solid line) and phase in radians (dashed line) of the transmission coefficient of the designed superlens as a function of the transverse wave number. (a) $f=0.8996$ GHz, ideal components. (b) $f=0.91$ GHz, dissipation in the lumped components and in the substrate is taken into account.

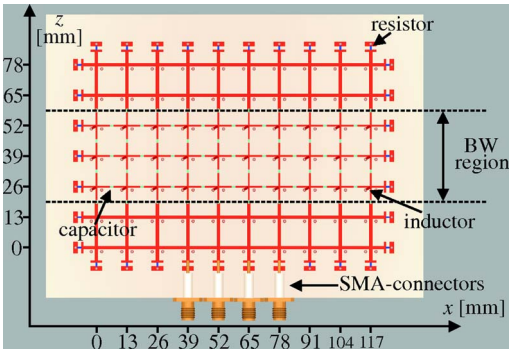

FIG. 5. (Color online) Two-dimensional prototype of the proposed structure (one horizontal layer of the designed 3D structure).

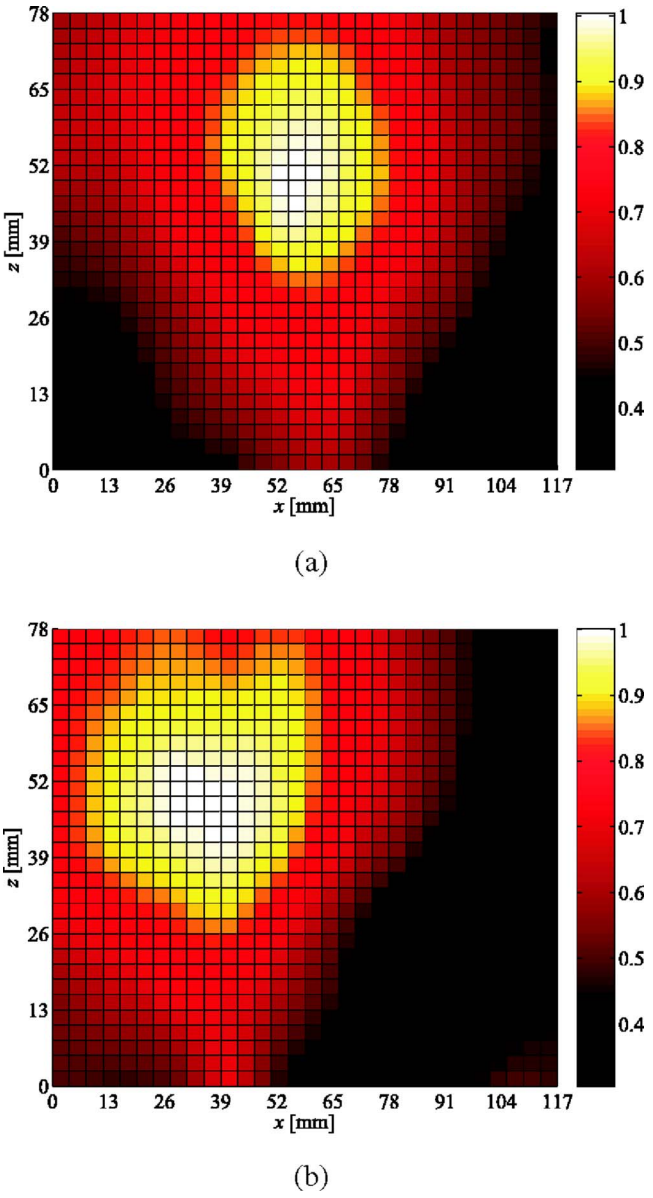

FIG. 6. (Color online) Measured amplitude of the vertical component of electric field on top of the 2D structure at $f=900$ MHz. Fields are normalized to the maximum value. (a) Symmetrical excitation by two sources at $x=52$ mm, $z=-6.5$ mm and $x=65$ mm, $z=-6.5$ mm. (b) One source at $x=39$ mm, $z=-6.5$ mm.

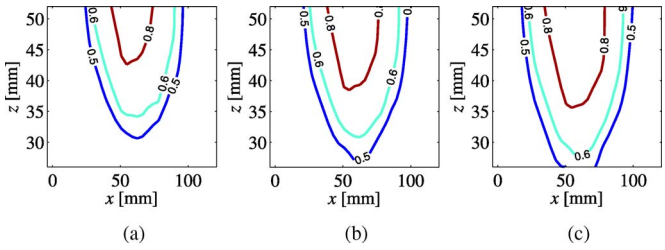

FIG. 7. (Color online) Time-harmonic electric field on top of the 2D structure at $f=900$ MHz. Fields are normalized to the maximum value. Symmetrical excitation by two sources at $x=52$ mm, $z=-6.5$ mm and $x=65$ mm, $z=-6.5$ mm. (a) $\phi=1$, (b) $\phi=1+\pi/20$, and (c) $\phi=1+2\pi/20$.

soldered to the strips and the outer conductors to the ground. The SMA connectors that were not used at each measurement were terminated with 50 Ω loads.

By connecting port 2 of a vector network analyzer to the excitation point(s) of the structure and port 1 to a probe antenna (a short vertical monopole antenna), the electric field distribution on top of the structure could be measured (by measuring S_{12}). The measured vertical component of the electric field is proportional to the voltages at the network nodes, a noninvasive direct measurement of which is a complicated task at 1 GHz. The probe antenna was connected to an automated measurement robot, which could be programed to position the probe at certain points. Here the field was measured at the center of each node of the structure which corresponds to 70 measurement points. The BW region is situated in the area 19.5 mm $<z<$ 58.5 mm. See Fig. 6 for the measured electric field distributions on top of the structure. Two sources are used in Fig. 6(a) to obtain the symmetrical excitation of the structure.

As is seen in Figs. 6(a) and 6(b), the maximum values of the amplitude occur at the back edge of the BW region, as it is expected from the theory. In Fig. 6(b) the point of excitation is displaced from the middle to show that the observed effects are not caused by reflections from the side edges. It is clear that both propagating and evanescent modes are excited in the structure, because the fields do not experience significant decay in the first FW region (evanescent modes decay exponentially) and there is a remarkable growth of the amplitude in the BW region (only evanescent modes can be "amplified" in a passive structure like this). The experiment does not show any noticeable reflections at the FW/BW interfaces, which implies a good impedance matching between the two networks.

To show that the structure supports backward waves, the time-harmonic electric field was plotted from the measured complex field using

$$E_{\text{real}} = \text{Re}\{E_{\text{complex}} e^{j\omega t}\}. \tag{3}$$

When the field plot is animated as a function of time, it is seen that the waves propagate "backward" (towards the point of excitation) in the BW region. To illustrate this effect, some contour lines of the time-harmonic field are plotted in Fig. 7 with different values of the phase angle ($\phi=\omega t$).

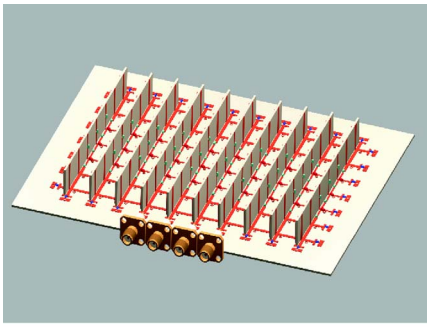

(a)

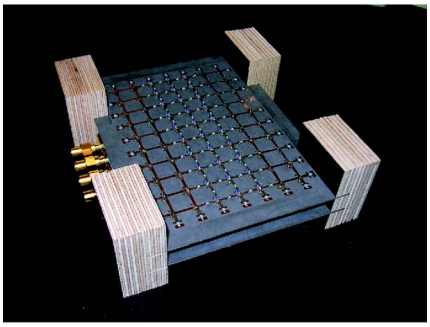

(b)

FIG. 8. (Color online) (a) Geometry of the 3D structure (one horizontal layer and ten vertical sublayers shown). (b) Experimental prototype of the 3D structure with two horizontal layers.

V. THREE-DIMENSIONAL REALIZATION

To realize a three-dimensional structure, a second two-dimensional layer as in Sec. IV was manufactured. To connect these two layers, ten vertical sublayers of height of 12.2 mm were soldered between them. See Fig. 8(a) for the geometry of the structure (one horizontal layer and ten vertical sublayers are shown). The resulting 3D structure is isotropic with respect to waves propagating inside the TLs (distance between adjacent horizontal and vertical nodes remains

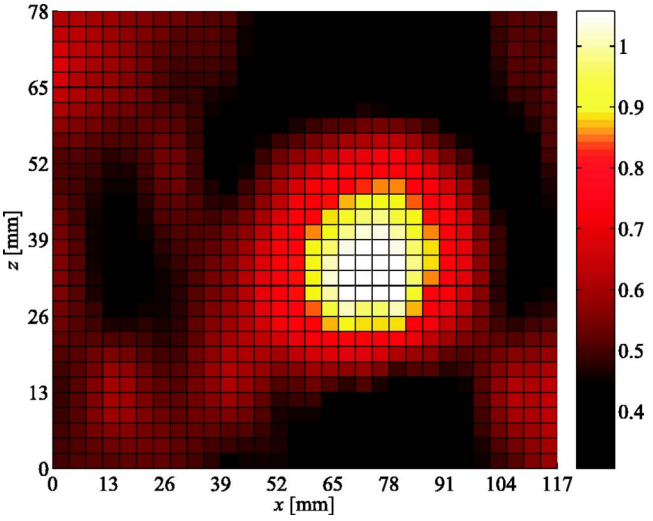

FIG. 9. (Color online) Measured amplitude of the vertical component of electric field on top of the 3D structure (two horizontal layers) at $f=900$ MHz. Fields are normalized to the maximum value. One source below the lower horizontal layer at $x=78$ mm, $z=39$ mm.

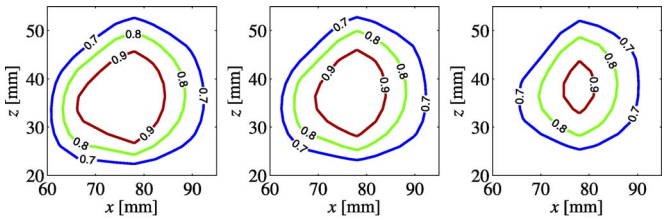

FIG. 10. (Color online) Time-harmonic electric field on top of the 3D structure (two horizontal layers) at $f=900$ MHz. Fields are normalized to the maximum value. One source below the lower horizontal layer at $x=78$ mm, $z=39$ mm. (a) $\phi=1.2$, (b) $\phi=1.2+\pi/20$, and (c) $\phi=1.2+2\pi/20$.

the same and the vertical microstrip lines are also loaded with capacitors in the BW region). A photograph of the manufactured two-layer structure is shown in Fig. 8(b).

Having more than one layer in the structure, wave propagation along the vertical axis (the y axis) can be experimentally tested. This was done by exciting the structure from the bottom of the lower horizontal layer at $x=78$ mm, $z=39$ mm (this point is inside the BW region, as can be seen from Fig. 5). See Fig. 9 for the electric field distribution measured on top of the upper layer and Fig. 10 for the instantaneous electric field snapshots. Figure 9 proves the three-dimensional isotropy of the proposed network that was predicted theoretically.[13] Figure 10 demonstrates the backward-wave propagation, because the point of the source appears to be a "sink" for moving contours of instantaneous values of the electric field.

Next, a third layer as in Sec. IV was manufactured and appended on top of the other two horizontal layers using vertical sublayers, as shown in Fig. 8(a). A photograph of the manufactured three-layer structure is shown in Fig. 11. The structure was again excited using the same connectors as in Sec. IV (situated now in the lowest horizontal layer). The electric field distribution on top of the upper layer was measured as in Sec. IV. See Fig. 12 for the measured electric field distribution on top of the structure.

As is seen in Fig. 12, the maximum field value occurs near the back edge of the BW region. Vertical propagation in the BW region was verified as in the case of two horizontal layers and similar results as in Figs. 9 and 10 were obtained.

VI. CONCLUSIONS

In this paper we have described the realization and testing of a three-dimensional transmission-line network which

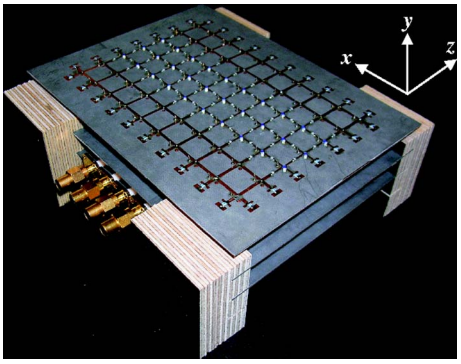

FIG. 11. (Color online) Experimental prototype of the 3D structure with three horizontal layers.

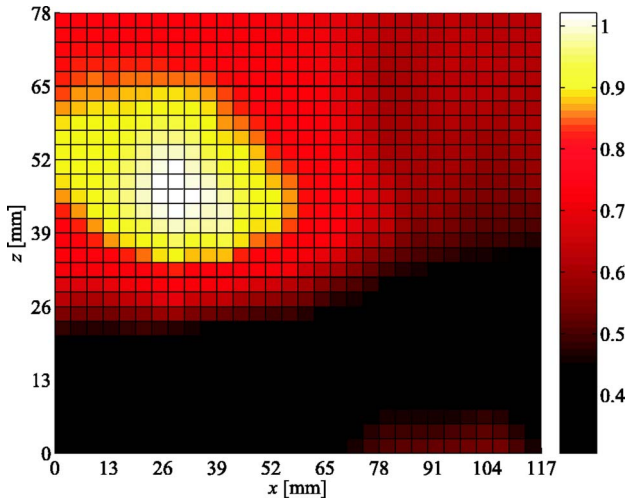

FIG. 12. (Color online) Measured amplitude of the vertical component of electric field on top of the 3D structure (three horizontal layers) at $f=900$ MHz. Fields are normalized to the maximum value. One source at $x=39$ mm, $z=-6.5$ mm, situated in the bottom layer.

is a circuit analogy of the superlens proposed by Pendry. The backward-wave slab, which is the key part of this superlens, is implemented by loading a three-dimensional transmission-line network with lumped inductive and capacitive components. A prototype of the proposed structure has been built. Backward-wave propagation and amplification of evanescent waves in the structure have been verified by measurements. Detailed theoretical analysis of such structure is given in Ref. 13.

ACKNOWLEDGMENTS

This work has been done within the frame of the *Metamorphose* Network of Excellence and partially funded by the Academy of Finland and TEKES through the Center-of-Excellence program. The authors would like to thank Dr. Mikhail Lapine for helpful discussions.

[1] J. B. Pendry, Phys. Rev. Lett. **85**, 3966 (2000).
[2] V. G. Veselago, Sov. Phys. Usp. **10**, 509 (1968).
[3] S. I. Maslovski and S. A. Tretyakov, J. Appl. Phys. **94**, 4241 (2003).
[4] S. I. Maslovski, S. A. Tretyakov, and P. Alitalo, J. Appl. Phys. **96**, 1293 (2004).
[5] D. R. Smith, W. J. Padilla, D. C. Vier, S. C. Nemat-Nasser, and S. Schultz, Phys. Rev. Lett. **84**, 4184 (2000).
[6] R. A. Shelby, D. R. Smith, and S. Schultz, Science **292**, 77 (2001).
[7] C. G. Parazzoli, R. B. Greegor, K. Li, B. E. C. Koltenbah, and M. Tanielian, Phys. Rev. Lett. **90**, 107401 (2003).
[8] G. V. Eleftheriades, A. K. Iyer, and P. C. Kremer, IEEE Trans. Microwave Theory Tech. **50**, 2702 (2002).
[9] L. Liu, C. Caloz, C.-C. Chang, and T. Itoh, J. Appl. Phys. **92**, 5560 (2002).
[10] C. Caloz and T. Itoh, IEEE Trans. Antennas Propag. **52**, 1159 (2004).
[11] A. Grbic and G. V. Eleftheriades, Phys. Rev. Lett. **92**, 117403 (2004).
[12] A. Sanada, C. Caloz, and T. Itoh, IEEE Trans. Microwave Theory Tech. **52**, 1252 (2004).
[13] P. Alitalo, S. Maslovski, and S. Tretyakov, J. Appl. Phys. **99**, 064912 (2006).
[14] A. Grbic and G. V. Eleftheriades, J. Appl. Phys. **98**, 043106 (2005).
[15] W. J. R. Hoefer, P. P. M. So, D. Thompson, and M. M. Tentzeris, IEEE MTT-S Int. Microwave Symp. Dig. 313 (2005).